# We are IntechOpen, the world's leading publisher of Open Access books
# Built by scientists, for scientists

## 6,900
Open access books available

## 186,000
International authors and editors

## 200M
Downloads

Our authors are among the

## 154
Countries delivered to

## TOP 1%
most cited scientists

## 12.2%
Contributors from top 500 universities

CLARIVATE ANALYTICS
**BOOK CITATION INDEX**
INDEXED

**WEB OF SCIENCE**™

Selection of our books indexed in the Book Citation Index
in Web of Science™ Core Collection (BKCI)

# Interested in publishing with us?
# Contact book.department@intechopen.com

Numbers displayed above are based on latest data collected.
For more information visit www.intechopen.com

# Interaction of Copper Alloys with Hydrogen

I. Peñalva[1], G. Alberro[1], F. Legarda[1],
G. A. Esteban[1] and B. Riccardi[2]
*[1]University of the Basque Country (UPV/EHU),*
*Dept. Nuclear Engineering & Fluid Mechanics,*
*Faculty of Engineering, Bilbao,*
*[2]Fusion for Energy, Barcelona,*
*Spain*

## 1. Introduction

Copper alloys are well known for their electrical and thermal conductivity, good resistance to corrosion, ease of fabrication and good strength and fatigue resistance. These properties make copper alloys suitable for several electrical and heat-conduction industrial applications. However, many of these industrial processes deal with hydrogen, and the interaction of this gas with copper alloys may affect to their mechanical features. Hydrogen dissolves in all metals to some extent. The dissolved hydrogen in the bulk of the material may change its mechanical properties assisting in its fracture, for example, and leading the material to the so-called hydrogen embrittlement. Therefore, it becomes important to characterise the transport properties of hydrogen in copper alloys as well as their ability to migrate by diffusion through structural walls by interstitial dissolution and trapping. This characterisation allows the improvement of the aforementioned industrial applications.

Lately, copper alloys are being considered as a technical option to construct a pipeline to transport any gaseous fuel including those of high hydrogen content or even pure hydrogen. In relation to this matter, the evaluation of hydrogen migration through the wall of the pipeline and the definition of related fundamental physics are key-issues when performing any risk evaluation because of hydrogen leak capacity. Apart from this question, it is well known the ability of hydrogen to damage copper alloys at high temperatures when they contain oxygen, this problem being directly connected to the ability of hydrogen to migrate through the solid material.

The research in nuclear fusion technology is also highly interested in copper materials. In fact, copper alloys have been selected as structural/heat sink materials that may be used in future fusion reactors like ITER because of their high thermal conductivity, good mechanical properties, thermal stability at high temperature and good resistance to irradiation-induced embrittlement and swelling. In this research area, heat sink/structural materials are subjected to high heat flux and, therefore, must possess a combination of high thermal conductivity and high mechanical strength. Apart from the previous properties, the interaction of hydrogen isotopes with copper alloys that could be part of the in-vessel components of a fusion reactor is of primary importance because it affects to the fuel

economy, the plasma stability and the radiological safety of the facility. There are various examples of predictive works trying to establish the time dependant evolution of migration fluxes and fuel inventory within fusion reactor components (Esteban et al., 2004; Meyder et al., 2006) by means of numerical simulation codes that use the hydrogen transport and trapping properties as the main input parameters. Trapping is the process by which dissolved hydrogen atoms remain bound to some specific centres known as "traps" (e.g. inclusions, dislocations, grain boundaries and precipitates). Hence, hydrogen isotopes may be dissolved in trapping or lattice sites of the material. The effect of trapping on hydrogen transport affects to the transport parameters and also to the physical and mechanical properties of the copper alloys involved.

Two of the most promising copper alloys at the present time in several specialised research areas are oxide dispersion strengthened (DS) copper alloys and precipitation hardened (PH) copper alloys (Barabash et al., 2007; Fabritsiev & Pokrovsky, 2005; ITER, 2001; Lorenzetto et al., 2006; Zinkle & Fabritsiev, 1994). This chapter will analyse and compare the experimental hydrogen transport parameters of diffusivity, permeability and Sieverts' constant for the diffusive regime of these kinds of copper alloys. Results can then be extrapolated as general behaviour for similar copper alloys. Trapping properties will also be discussed. Data shown in the chapter will refer to real experimental values for copper alloys obtained by means of the gas evolution permeation technique.

## 2. Experimental

The gas evolution permeation technique is widely used to characterize the hydrogen transport in metallic materials and, therefore, it turns out to be a suitable technique for the analysis of hydrogen transport in specimens made of different copper alloys. Oxide dispersion strengthened (DS) copper alloys and precipitation hardened (PH) copper alloys have been characterized by means of this experimental method. More precisely, experimental hydrogen transport data are available for a DS copper alloy named GlidCop® Al25 and for a PH-CuCrZr copper alloy named ELBRODUR®.

### 2.1 Dispersion strengthened and precipitation hardened copper alloys

The GlidCop® Al25 copper alloy is produced by OMG America and contains wt. 0.25 % Al in the form of $Al_2O_3$ particles. The material is manufactured by means of powder metallurgy using Cu-Al alloy and copper oxide powders. These are mixed and heated to form alumina and then consolidated by hot extrusion. This fabrication method derives in a high density of homogeneously distributed $Al_2O_3$ nanometric particles within the elongated grain substructure of the material, which are thermally stable and resistant to coarsening so that the grain substructure is resistant to thermal annealing effects (Esteban et al., 2009).

The ELBRODUR® copper alloy is produced by KME-Germany AG. The alloy composition is wt. 0.65 % Cr, wt. 0.05 % Zr and the rest Cu. The fabrication process and the heat treatment consisting of solution annealing (1253 K, 1 h), water quenching and aging (748 K, 2 h) makes possible the presence of nanometric Guinier-Preston zones and incoherent pure Cr particles that provide the material with the high mechanical strength by dislocation motion inhibition. An image of the CuCrZr microstructure is shown in *Figure 1*.
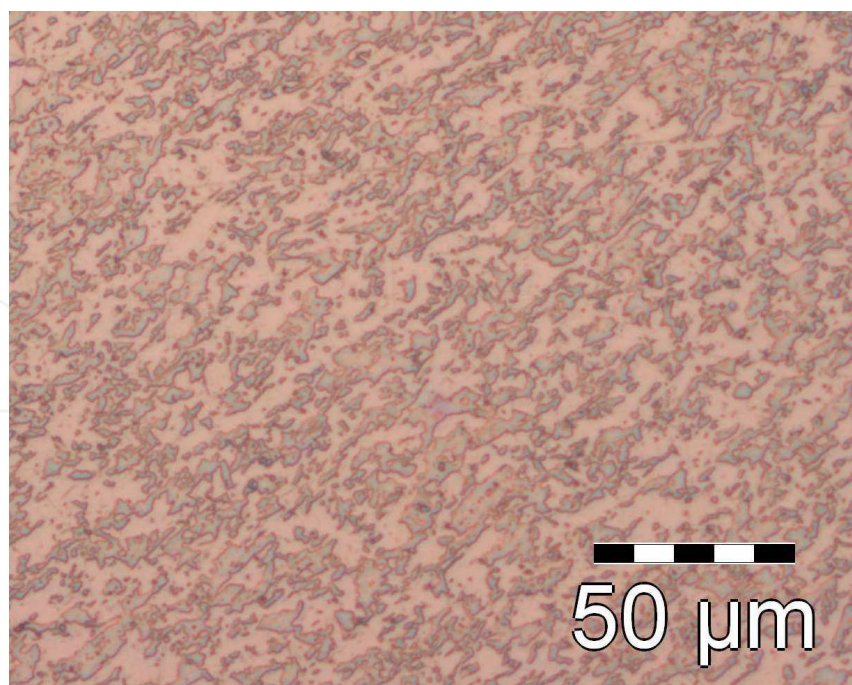
Fig. 1. CuCrZr microstructure.

## 2.2 Gas evolution permeation technique

A schematic view of a permeation facility is shown in *Figure 2*. The physical principle of the experimental technique entails the gas flux recording that passes through a thin membrane of the material of interest from a high gas pressure region to a low-pressure region at initial vacuum conditions.

The hydrogen migration through the specimen is measured by recording the pressure increase with time in the low-pressure region with two capacitance manometers (Baratron MKS Instr.-USA) P1 and P2 with full scale range of 1000 Pa and 13.33 Pa respectively. An electrical resistance furnace (F) regulated by a PID controller allows to establish the sample temperature within a +/- 1 K precision. The temperature of the specimen is measured by a Ni-Cr/Ni thermocouple inserted into a well drilled in one of the two flanges where the specimen is mounted. The pressure controller (PC) allows the instant exposure of the high-pressure face of the specimen to any desired gas driving pressure, which is measured by means of a high-pressure transducer (HPT).

Before any experimental test is performed with high purity hydrogen (99.9999%), ultra-high vacuum state is reached inside the experimental volumes (up to $10^{-7}$ Pa) in order to assure the absence of any deleterious species (such as oxygen or water vapour) that may provoke surface oxidation of the specimen (S). There are three ultra-high vacuum pumping units, UHV, composed by a hybrid turbomolecular pump and a primary pump; they pump down the inner volumes of the rig to the desired vacuum level with the help of heating tapes. The vacuum state is checked with three Penning gauges PG in different zones of the facility. A quadrupole mass spectrometer (QMS) is available to check the purity of the gas before and after any experimental test and as an alternative means of testing the quality of the vacuum.
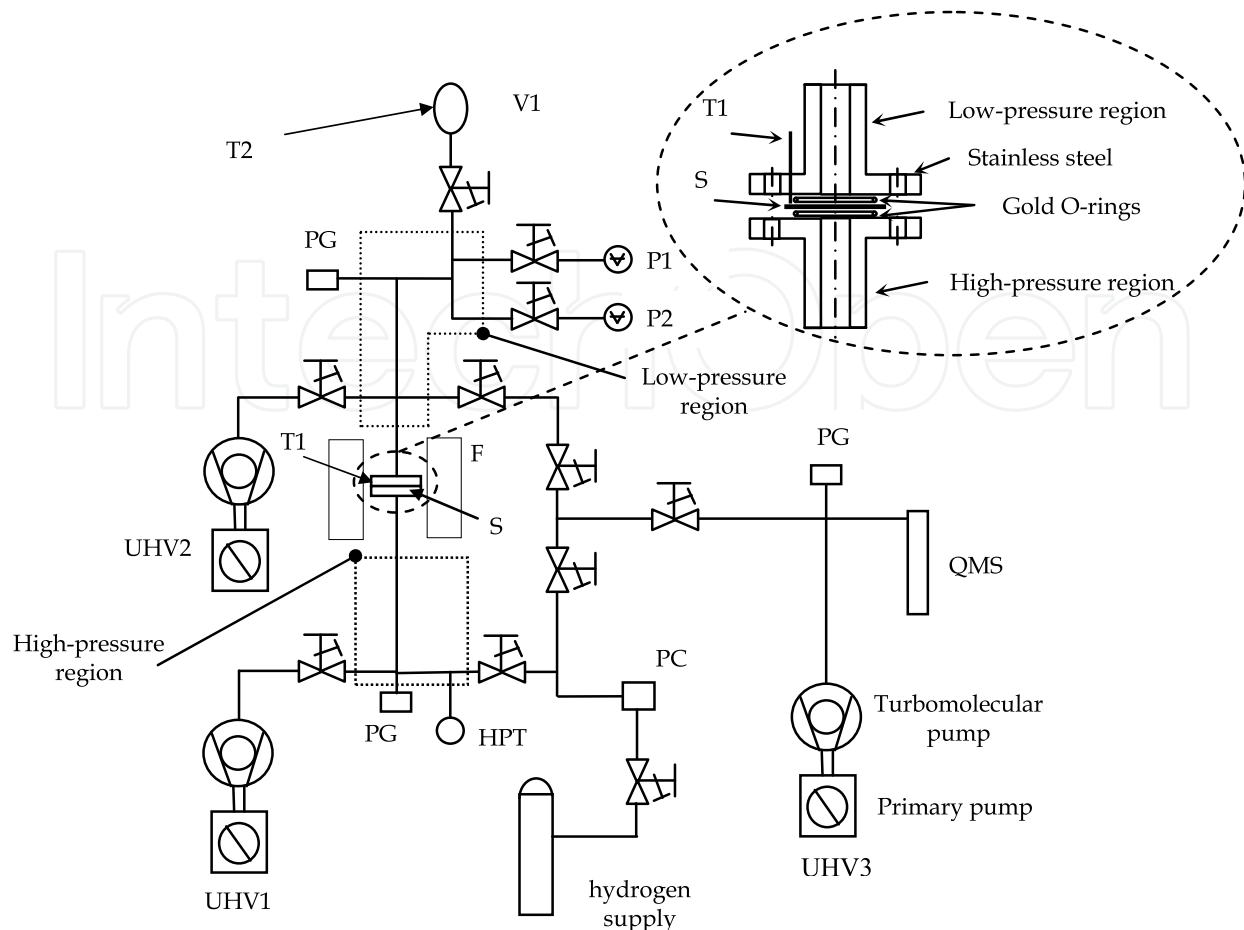
Fig. 2. Schematic view of the permeation facility. PG – Penning gauge; F – furnace; PC – pressure controller; HPT – high-pressure transducer; QMS – quadrupole mass spectrometer; S – specimen; T1, T2 – nickel/chromium-nickel thermocouples; P1, P2 – capacitance manometers; UHV – ultra-high vacuum pumping units, V1 – calibrated volume.

In an individual experimental test, the high driving pressure starts forcing permeation through the high-pressure face of the specimen towards the low-pressure region, where the hydrogen permeation flux rises progressively with time until a steady-state permeation flux is reached. After every experimental permeation run, an expansion of the gas in the low-pressure region is performed to a calibrated volume (V1) in order to convert pressure values into permeated gas amount, or alternatively, the speed of pressure increase into permeation flux. The modelling of the pressure increase $p(t)$ due to the gas permeation towards the low-pressure region (a typical experimental permeation curve is shown in *Figure 3*) makes possible to obtain the hydrogen transport properties of the copper alloy: permeability ($\Phi$), diffusivity ($D$) and Sieverts´ constant ($K_S$).

The permeated flux under diffusive regime for every temperature depends on the thickness of the sample, the values of the loading pressure and the permeability of the gas ($\Phi$). This transport parameter defines the gas-material interaction. Diffusion is a physical property that allows the flux of a gas through the bulk of a solid material due to, in this case, a concentration gradient of the dissolved hydrogen. The gas flux in the bulk of the material depends on the concentration gradient and on the temperature. The proportionality

between the flux and the concentration gradient is called diffusivity ($D$) and is directly related to the kinetics of the system in order to reach the equilibrium by means of diffusion. Finally, Sieverts´ constant ($K_S$) is directly related to the solubility of the gas in the solid and can be derived from the values of diffusivity and permeability.
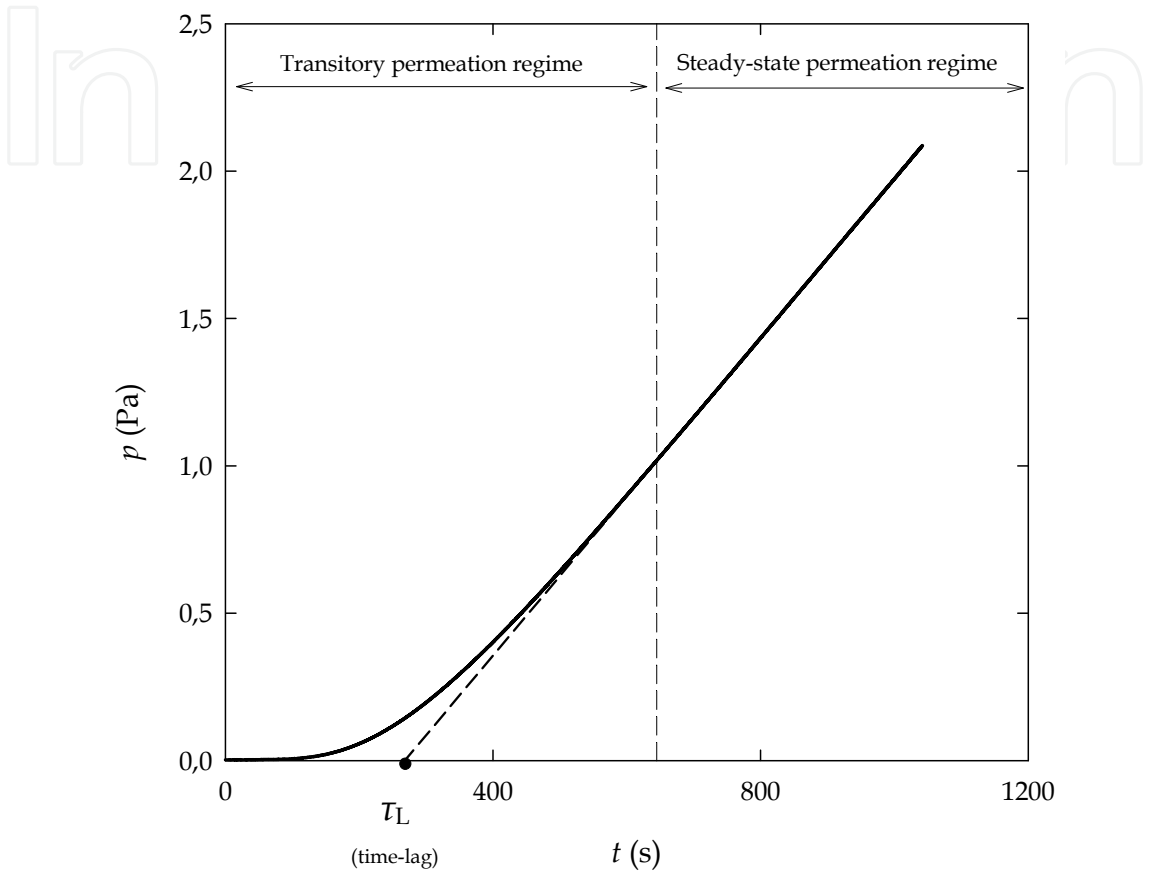


Fig. 3. Experimental permeation curve: transitory permeation regime and steady-state permeation regime. Definition of the time-lag.

## 3. Theory

Typical bulk parameters for the study of hydrogen transport in metal lattices are the diffusivity ($D$), the Sieverts´ constant, ($K_S$), and the permeability ($\Phi$) (Alberici & Tominetti, 1995). The diffusivity is related to the diffusing flux in a metallic matrix, $J$, and the gradient of the gas concentration in the matrix, $\nabla c$, by the first Fick's law:

$$J = -D \cdot \nabla c \tag{1}$$

where is easy to see that $D$ is linked to the migration velocity of the gas in the material.

In this equation, taking into account a homogeneous bulk, $D$ will be supposed to be uniform and constant throughout the material volume and it only depends on the absolute temperature, $T$, by an Arrhenius relationship:

$$D = D_0 \cdot \exp(-E_d / R \cdot T) \tag{2}$$

where $E_d$ is the diffusion activation energy, which is always positive.

Experimentally it is found that hydrogen dissolves atomically in metal lattices; the proportionality between the atomic gas concentration in the bulk volume, $c$, and the square root of the equilibrium gas pressure outside the bulk, $p^{1/2}$, is known as the Sieverts´ constant:

$$K_S = c / \sqrt{p} \tag{3}$$

It is interesting to note that Sieverts´ constant also shows an Arrhenius dependence on the temperature:

$$K_S = K_{S,0} \cdot \exp(-E_s / R \cdot T) \tag{4}$$

where $E_S$ is the activation energy for solution, which can be either positive or negative.

Permeability ($\Phi$) is given by means of Richardson's law that states a linear relation between $D$ and $K_S$:

$$\phi = K_S \cdot D \tag{5}$$

From Eq. 5, it is obvious that permeability also follows an Arrhenius behaviour like $D$ and $K_S$, with an activation energy of permeation which is the sum of $E_d$ and $E_s$:

$$\phi = \phi_0 \cdot \exp(-(E_d + E_s) / R \cdot T) \tag{6}$$

All the processes involved in the interaction between hydrogen and the metallic material, either on the surface or in the bulk, may be explained by the analysis of the different potential energy levels acquired by the hydrogen atom/molecule in the immediacy of, and within the metal (Esteban et al., 1999). These energy levels are summarised in *Figure 4* (Möller, 1984). Out of the material, hydrogen is in the molecular form: the solid line refers to atomic hydrogen and the broken line to molecular hydrogen. All the energy increments and decrements depicted in *Figure 4* define the hydrogen behaviour within, and in the vicinity of the solid metal and explain observed physical processes. The dissociation energy, $E_{di}$, is the amount of energy needed for splitting a hydrogen molecule into two atoms. The chemisorption energy, $E_{ch}$, refers to the chemical binding established between atomic hydrogen and metallic atoms. The adsorption energy, $E_{ad}$, is the energy barrier hydrogen has to surmount in order to access to a chemisorption site and it depends on the surface condition. The solution energy, $E_s$, is the energy difference between a free atom and a dissolved one and depending on the sign of this energy the material is characterised as endothermic, $E_s > 0$, or exothermic, $E_s < 0$. The diffusion energy, $E_d$, is the barrier the diffusing atom has to surmount in order to pass, within the lattice, from one solution site to another. The trapping energy, $E_t$, is the potential well to which a hydrogen atom remains bound when interacting with the potential trapping sites. $\Delta E$ states for the energy difference between a normal solution site and a trapping site, $(E_s – E_t)$. Finally, $E_c$ states for the energy difference when comparing potential barriers between normal solution sites and a trapping site.

Fig. 4. Potential energy distribution in a metal (Möller, 1984).

Hydrogen isotope transport through material may be limited either by gas interstitial diffusion through the bulk (diffusion-limited regime) or by the physical-chemical reactions of adsorptive dissociation and desorptive recombination occurring on the surface of the solid material (surface-limited regime). The objective of this experimental task is usually to characterize the diffusion-limited regime instead of the surface-limited regime, the second one being only relevant when any kind of impurities or oxides are present on the surface of the material.

"Trapping" is the process by which dissolved hydrogen atoms remain bound to some specific centres known as "traps" (e.g. inclusions, dislocations, grain boundaries and precipitates). Hence, hydrogen isotopes may be dissolved in trapping or lattice sites of the material. The effect of trapping on hydrogen transport is, on the one hand, the increase in the gas absorbed inventory, i.e. the increase in the effective Sieverts' constant ($K_{S,eff}$) with respect to the aforementioned lattice Sieverts' constant ($K_S$). On the other hand, the dynamics of transport becomes slower, i.e. the decrease of the effective diffusivity ($D_{eff}$) with respect to the aforementioned lattice diffusivity ($D$). As a result, the Arrhenius temperature dependence of the parameters remains modified as follows, according to Eqs. (2) and (4) for diluted solutions (Oriani R.A., 1970):

$$D_{eff} = \frac{D}{1 + \frac{N_t}{N_1}\exp(E_t / R \cdot T)}. \tag{7}$$

$$K_{S,eff} = K_S \cdot \left(1 + \frac{N_t}{N_1}\exp(E_t / R \cdot T)\right) \tag{8}$$

$D_0$ and $K_{S,0}$ being the pre-exponential lattice diffusivity and pre-exponential lattice Sieverts' constant, and $E_d$, $E_s$ the diffusion and solution energies, respectively. $N_t$ (m$^{-3}$) is the trap sites concentration, $N_l$ (m$^{-3}$) is the lattice dissolution sites concentration and $E_t$ the trapping energy.

When the individual effective parameters for each experimental temperature have been obtained, another fitting routine is separately run with Eqs. (2), (4), (7) and (8) for the lattice parameters $D_0$, $E_d$, $K_{S,0}$ and $E_s$ and trapping parameters $E_t$ and $N_t$ over the correspondent temperature range of influence. The value of $8.5 \cdot 10^{28}$ m$^{-3}$ is taken for the density of solution sites into the lattice $N_l$, assuming that the copper alloy is close to a fcc structure where hydrogen occupies only the octahedral interstitial positions (Vykhodets et al., 1972).

The effective transport parameters of diffusivity ($D_{eff}$) and permeability ($\Phi$) are evaluated for each temperature by modelling the experimental permeation curves obtained for every individual test. The Sieverts' constant ($K_{S,eff}$) is derived from the definition of permeability that states the relationship amongst the three transport parameters:

$$\Phi = D_{eff} \cdot K_{S,eff} \tag{9}$$

A subsequent analysis of the Arrhenius dependence of these transport parameters with temperature enables the obtaining of the characteristic transport parameters of trapping energy ($E_t$) and density of traps ($N_t$).

The obtaining of the theoretical expression for the pressure increase with time in the low-pressure region as a function of the previous transport parameters is briefly explained hereafter.

The specimens are thin discs with a very high ratio of the circular surface exposed to the gas in relation to the length of the diffusion path through the bulk of material. This is the reason why the problem can be modelled by an infinite slab with gas diffusion occurring in the direction perpendicular to the surface of the specimen.
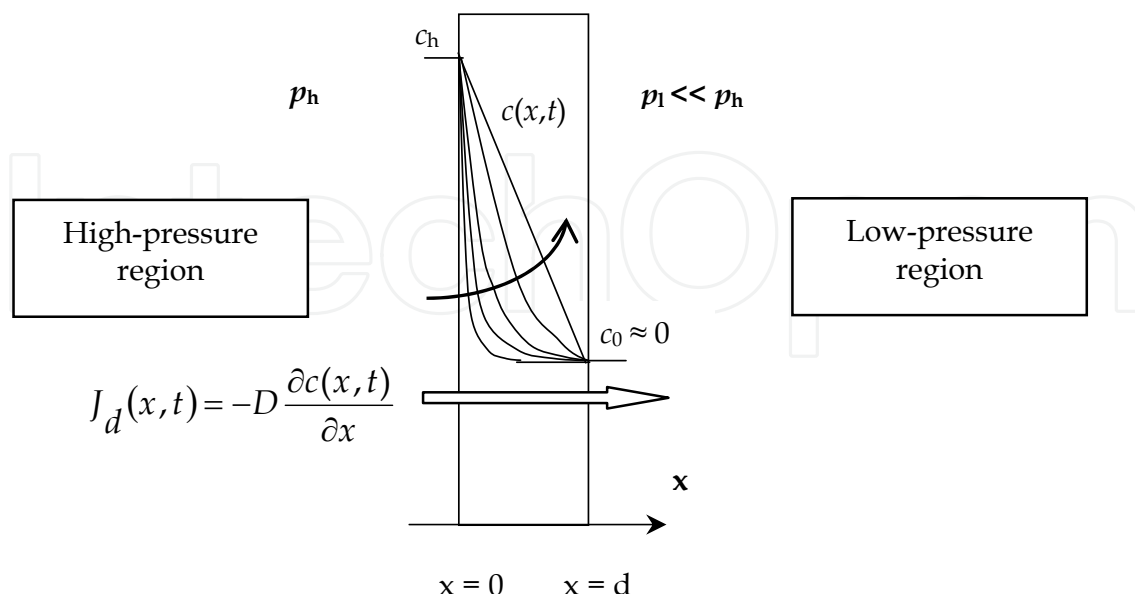


Fig. 5. Scheme of the permeation process through a 1-D slab. $p_h$ – high-pressure; $p_l$ – low-pressure; $d$ – thickness of the slab; $J_d$ ($x,t$) – diffusive flux; $c(x,t)$ – gas concentration.

A scheme of the gas transport through a sheet of material with a certain thickness ($d$) is shown in *Figure 5*. That specimen is exposed on one side to a certain gas driving pressure ($p_h$), whereas the other side is left under vacuum conditions (i.e. very low pressure $p_l$).

The hydrogen concentration ($c(x,t)$) at each position ($x$ coordinate) and each time ($t$) may be determined by solving the second Fick's law in the one dimension slab:

$$\frac{\partial c(x,t)}{\partial t} = D_{eff} \frac{\partial^2 c(x,t)}{\partial x^2} \tag{10}$$

The boundary conditions being the following:

- 1st condition: $c(x=0,t) = c_h$ , from the beginning, in the region closest to the surface, the gas concentration acquires the final equilibrium value in the saturation state given by Sieverts' law,

$$c_h = K_{S,eff} \cdot p_h^{0.5} \tag{11}$$

- 2nd condition: $c(x=d,t) = 0$ , the gas concentration in the low-pressure side is negligible in comparison to $c_h$; i.e. $p_l$ negligible in comparison to $p_h$,

$$c_0 = K_{S,eff} \cdot p_l^{0.5} \tag{12}$$

The initial condition is $c(x>0, t=0) = 0$; at the beginning of the test, the specimen is under vacuum conditions without any amount of hydrogen dissolved into the material.

The analytical solution of the Eq. (10) with the previous boundary and initial conditions is (Carslaw & Jaeger, 1959):

$$c(x,t) = c_h \left( 1 - \frac{x}{d} \right) - \frac{2c_h}{\pi} \sum_{n=1}^{\infty} \frac{1}{n} \sin\left( \frac{n \cdot \pi \cdot x}{d} \right) \exp\left( -D_{eff} \frac{n^2 \cdot \pi^2}{d^2} t \right) \tag{13}$$

The resultant flux to the low-pressure region can be evaluated as:

$$J(x=d,t) = -D \frac{\partial c(x,t)}{\partial t} \bigg|_{x=d} = \frac{D_{eff} \cdot K_{S,eff} \cdot p_h^{0.5}}{d} \left[ 1 + 2\sum_{n=1}^{\infty} (-1)^n \exp\left( -D \frac{n^2 \cdot \pi^2}{d^2} t \right) \right] \tag{14}$$

The total gas inventory ($I(t)$) permeated to the low-pressure region is evaluated by accounting for all the gas flux released during the considered time period ($t$) and taking into account the surface area of the specimen ($A_s$):

$$I(t) = A_s \int_0^t J(d,t') \, dt' = \frac{\Phi \cdot p_h^{0.5}}{d} A_s \cdot t - \frac{\Phi \cdot p_h^{0.5} \cdot d}{6 \cdot D_{eff}} A_s -$$
$$\frac{2 \cdot \Phi \cdot p_h^{0.5} \cdot d}{6 \cdot D_{eff}} A_s \sum_{n=1}^{\infty} \frac{(-1)^n}{n^2} \exp\left( -D_{eff} \frac{n^2 \cdot \pi^2}{d^2} t \right) \tag{15}$$

Taking into account the ideal gas approximation, pressure increment with time in the low-pressure region due to this amount of gas is:

$$p(t) = \frac{R \cdot T_{eff}}{V_{eff}} \left[ \frac{\Phi \cdot p_h^{0.5}}{d} A_s \cdot t - \frac{\Phi \cdot p_h^{0.5} \cdot d}{6 \cdot D_{eff}} A_s - \frac{2 \cdot \Phi \cdot p_h^{0.5} \cdot d}{6 \cdot D_{eff}} A_s \sum_{n=1}^{\infty} \frac{(-1)^n}{n^2} \exp\left( -D_{eff} \frac{n^2 \cdot \pi^2}{d^2} t \right) \right] \quad (16)$$

Where the $V_{eff}$ is the effective volume where the permeated gas is retained, $T_{eff}$ is the temperature of the volume and R is the ideal gas constant ($8.314 \, J \cdot K^{-1} \cdot mol^{-1}$). The volume $V_{eff}$ is precisely measured in each experimental permeation test by performing gas expansion to a calibrated volume.

When imposing a very large period of time ($t \rightarrow \infty$) in the previous expression the evolution of pressure with time for the steady-state permeation regime is obtained:

$$p_\infty(t) = \frac{R \cdot T_{eff}}{V_{eff}} \left( \frac{\Phi \cdot p_h^{0.5}}{d} A_s \cdot t - \frac{\Phi \cdot p_h^{0.5} \cdot d}{6 \cdot D_{eff}} A_s \right) \quad (17)$$

This expression corresponds to the steady-state flux,

$$J_\infty = \frac{\Phi \cdot p_h^{0.5}}{d} \quad (18)$$

obtained from Eq. (17); this is the linear tendency shown in *Figure 3* on the right-hand side. When the straight line is extended down to cross the abscise axis in the time co-ordinate a characteristic time known as time-lag is obtained:

$$\tau_L = \frac{d^2}{6 \cdot D_{eff}} \quad (19)$$

The value of permeability ($\Phi$) can be derived from the slope of the straight line in steady-state permeation regime (Eq. (17)) and the effective diffusivity ($D_{eff}$) can be derived from the value of the time-lag. Nevertheless, a non-linear least-squares fitting to all the experimental points of each single test has been preferred with the general expression (Eq. (16)) in both the steady-state region and the transitory region by considering the permeability ($\Phi$) and the diffusivity ($D_{eff}$) as the fitting parameters.

In any individual permeation test, the gas is on contact with a solid surface and the hydrogen concentration profile through the sample thickness rises, becoming linear and stable after certain period of time. In that final permeation process the relationship between steady-state flux ($J_\infty$) and the loading pressure ($p_h$) will be different depending whether the transport regime is diffusion-limited or surface-limited (Esteban et al., 2002):

$$J_\infty = \frac{\Phi}{d} \cdot p_h^{0.5} \text{ (diffusion-limited)} \quad (20)$$

$$J_\infty = \frac{1}{2} \cdot \sigma \, k_1 \cdot p_h \text{ (surface-limited)} \quad (21)$$

where $\sigma k_1$ is the adsorption rate constant. The experimental confirmation of one of these relationships is a method to decide the type of transport regime for modelling the experimental tests.

## 4. Results and discussion

This section reviews the available data in literature for oxide dispersion strengthened (DS) copper alloys and precipitation hardened (PH) copper alloys. Results regarding interaction of these alloys with hydrogen are compared in relation to base material, Cu. Punctual experimental values are shown only for the ELBRODUR® alloy (not published), whereas Arrhenius regressions of the transport parameters are compiled for all the alloys.

Individual permeation tests have been carried out for the aforementioned copper alloys, GlidCop® Al25 (Esteban et al., 2009) and ELBRODUR®, with temperatures ranging from 573 K to 793 K and using loading pressures ranging from $10^3$ Pa to $1.0 \cdot 10^5$ Pa. Additionally, data for base material, Cu, (Reiter et al., 1993) and for a similar PH-CuCrZr alloy (Serra & Perujo, 1998) named ELBRODUR-II hereafter to distinguish from the material analysed, are also available. These results for the hydrogen transport parameters in copper alloys are summarised and discussed in the next paragraphs.

In relation to the permeation tests carried out for GlidCop® Al25 and ELBRODUR® copper alloys, the evaluation of the diffusive transport parameters has been assured because no surface effect has become relevant within the whole group of individual tests. This fact has been proved by studying the evolution of the experimental steady-state flux ($J_\infty$) with driving pressure ($p_h$) at the same temperature.

In the case of the ELBRODUR® copper alloy, a set of 9 permeation tests has been performed at the same temperature (688 K) with different loading pressures ($p_h$) in order to study the type of hydrogen transport regime. These results are shown in *Figure 6*. The exponential relationship between the steady-state hydrogen flux ($J_\infty$) and the loading pressure ($p_h$) has a power of $n = 0.52$, which is close to 0.5 (pure diffusion-limited regime) and far from 1.0 (pure surface-limited regime) (Eqs. (20) and (21), respectively).

Individual transport parameters of effective diffusivity ($D_{eff}$), permeability ($\Phi$) and effective Sieverts' constant ($K_{S,eff}$) have been obtained at different temperatures by modelling the corresponding individual permeation tests, both for GlidCop® Al25 (Esteban et al., 2009) and ELBRODUR®.

The dependence of the transport parameters on temperature for the ELBRODUR® copper alloy is shown in *Figure 7* (permeability), *Figure 8* (diffusivity) and *Figure 9* (Sieverts' constant), together with the results obtained for the aforementioned reference copper alloys (Esteban et al., 2009; Reiter et al., 1993; Serra & Perujo, 1998). The Arrhenius parameters are obtained by fitting the individual experimental values to the tendencies given by Eqs. (2), (4), (7) and (8), resulting:

$$\Phi \ (\mathrm{mol} \cdot \mathrm{m}^{-1} \cdot \mathrm{Pa}^{-0.5} \cdot \mathrm{s}^{-1}) = 2.38 \cdot 10^{-7} \cdot \exp(-73.9 \ (\mathrm{kJ} \cdot \mathrm{mol}^{-1}) / \mathrm{R} \cdot T)$$

$$D \ (\mathrm{m}^2 \cdot \mathrm{s}^{-1}) = 3.55 \cdot 10^{-5} \cdot \exp(-65.5 \ (\mathrm{kJ} \cdot \mathrm{mol}^{-1}) / \mathrm{R} \cdot T)$$

$$K_S \ (\text{mol} \cdot \text{m}^{-3} \cdot \text{Pa}^{-0.5}) = 6.71 \cdot 10^{-3} \cdot \exp(-8.4 \ (\text{kJ} \cdot \text{mol}^{-1}) / R \cdot T)$$

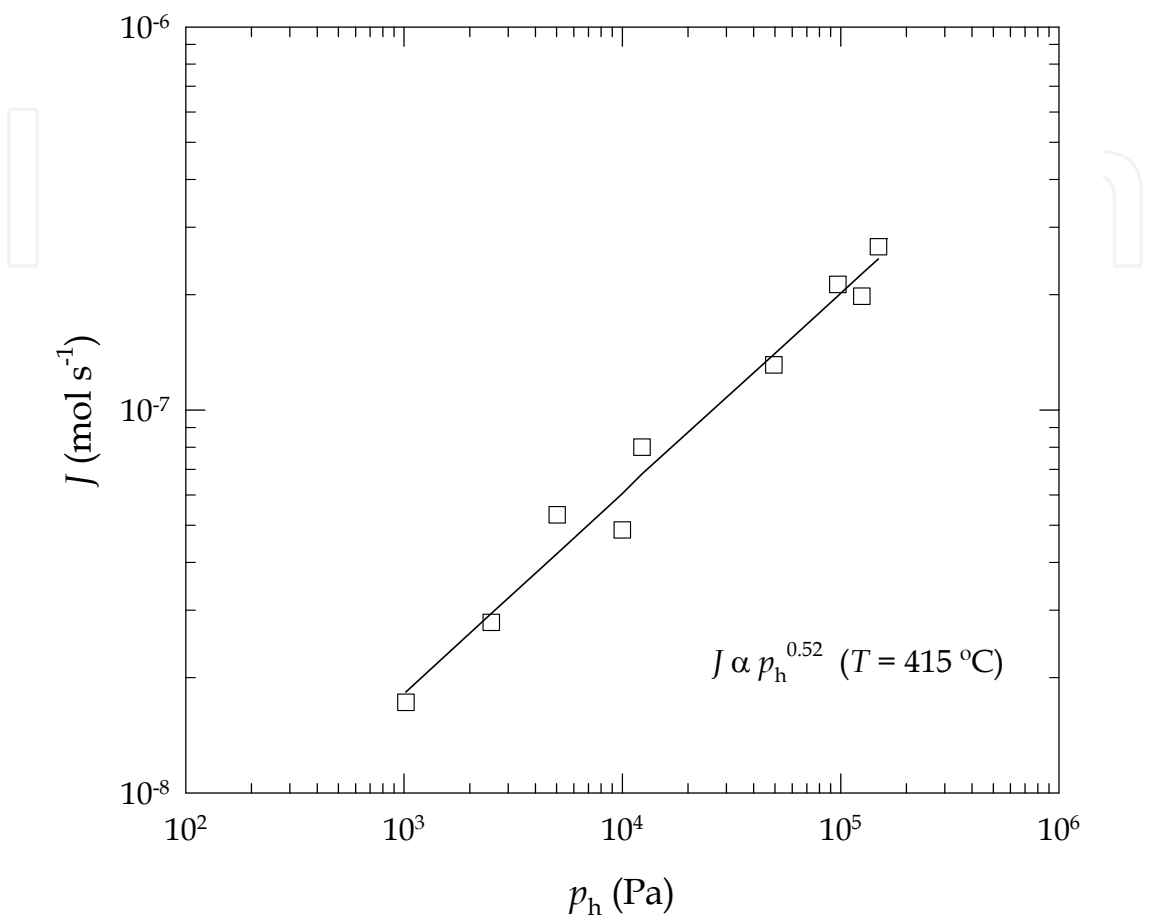The trapping parameters are $N_t = 3.7 \cdot 10^{24}$ m$^{-3}$ and $E_t = 51.2$ kJ mol$^{-1}$.



Fig. 6. Experimental hydrogen permeation steady-state flux in PH-CuCrZr alloy (ELBRODUR®) at 688 K and different driving pressures ranging from $10^3$ to $1.5 \cdot 10^5$ Pa.

The Arrhenius pre-exponentials and the activation energies of hydrogen transport parameters together with the trapping parameters that have been plotted in *Figs. 7-9* are shown in *Table 1*.

| Material (curve) | $\Phi_0$ | $E_\Phi$ | $D_0$ | $E_d$ | $K_{S0}$ | $E_S$ | $N_t$ | $E_t$ | $T$ |
|---|---|---|---|---|---|---|---|---|---|
| ELBRODUR (1) | 2.38·10⁻⁷ | 73.9 | 3.55·10⁻⁵ | 65.5 | 6.71·10⁻³ | 8.4 | 3.7·10²⁴ | 51.2 | 593-773 |
| GlidCop® Al-25 (2) (Esteban et al., 2009) | 5.87·10⁻⁷ | 80.6 | 5.70·10⁻⁵ | 76.8 | 0.006 | 3.7 | 3.1·10²² | 75.4 | 573-793 |
| ELBRODUR-II (3) (Serra & Perujo, 1998) | 5.13·10⁻⁷ | 79.8 | 5.70·10⁻⁷ | 41.2 | 0.90 | 38.6 | - | - | 553-773 |
| Cu (4) (Reiter et al, 1993) | 6.60·10⁻⁶ | 92.6 | 6.60·10⁻⁷ | 37.4 | 5.19 | 55.2 | - | - | 470-1200 |

Table 1. Experimental hydrogen transport parameters for reference copper alloys; $\Phi_0$ in mol·m⁻¹·Pa⁻⁰·⁵·s⁻¹, $E_\Phi$, $E_d$, $E_s$ and $E_t$ in kJ· mol⁻¹, $D_0$ in m²·s⁻¹, $K_{S0}$ in mol· m⁻³·Pa⁻⁰·⁵, $N_t$ in m⁻³ and $T$ in K.

There exists a marked difference between the transport parameters obtained in the PH-CuCrZr alloy (ELBRODUR®) in relation to the corresponding ones for the base material (Cu) (Reiter et al, 1993), DS copper alloy GlidCop® Al25 (Esteban et al., 2009), and a similar PH-CuCrZr alloy (Serra & Perujo, 1998) named ELBRODUR-II. There is a different metallurgical composition in the Zr content and a slight difference in the thermal treatment of both the ELBRODUR alloys. Moreover, in the work performed with ELBRODUR-II (Serra & Perujo, 1998) the effect of hydrogen trapping was not envisaged.

In the case of the transport property of permeability (*Figure 7*) the result obtained for the PHCuCrZr alloy ELBRODUR® is congruent with the results obtained in other reference Cu alloys. The permeation energy, 73.9 kJ/mol, preserves a similar value to those of the other Cu alloys (80.6 kJ/mol in GlidCop® Al25 and 79.8 kJ/mol in ELBRODUR-II) and it is slightly lower than that of the pure Cu (92.6 kJ/mol).

The aforementioned similar results in the four different materials are reasonable because permeability is a property describing the steady-state hydrogen migration through lattice with no influence of the trapping effect and the particular microstructural defects of each material; i.e. when enough period of time passes, hydrogen concentration dependence on depth adopts the final linear profile (see *Figure 5*) when trapping and detrapping (the inverse process) have reached equal equilibrium rates that cancel each other.
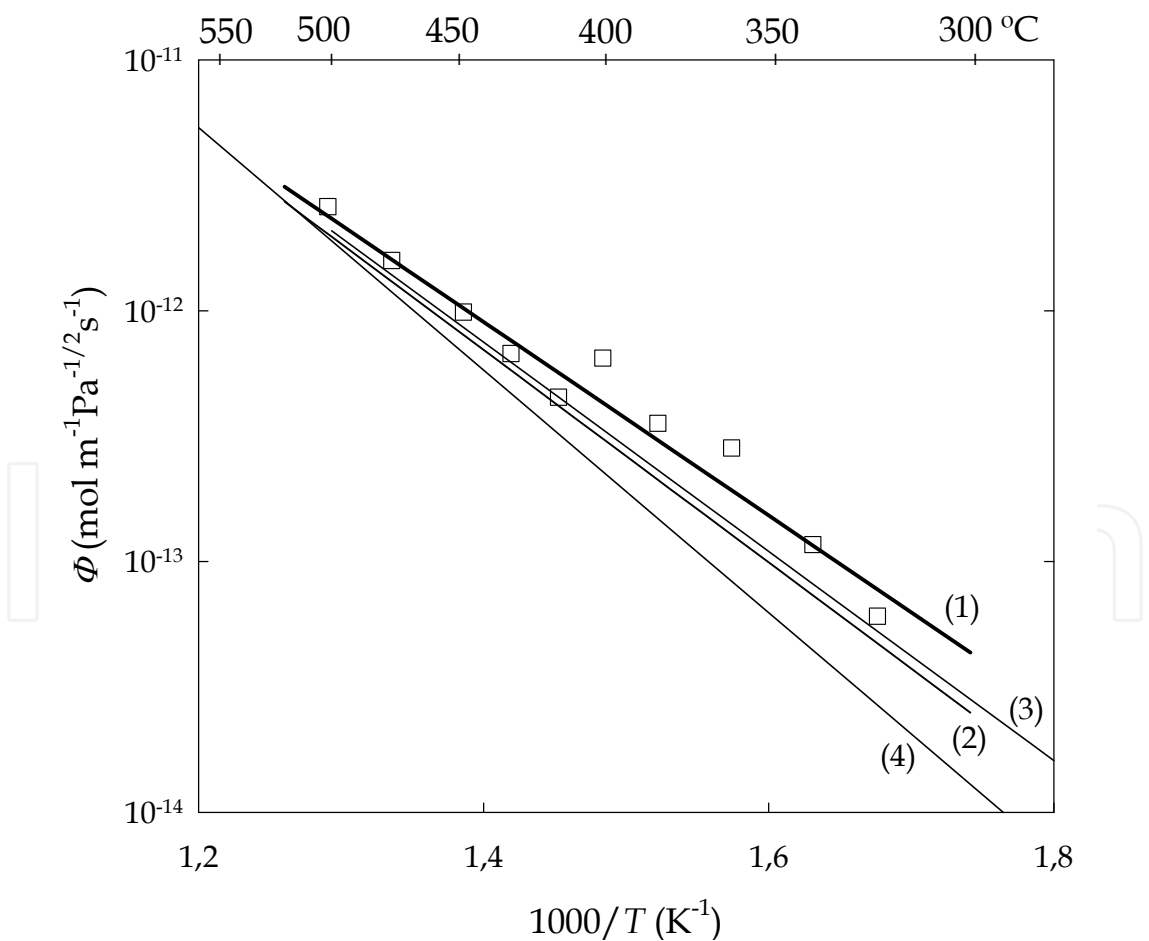


Fig. 7. Hydrogen permeability in PH-CuCrZr ELBRODUR® alloy compared with reference copper alloys: (1) ELBRODUR®, (2) GlidCop® Al25, (3) ELBRODUR-II, (4) pure Cu.

The influence of microstructural defects of the material acting as strong trapping sites for hydrogen absorption, can be observed in transport properties such as diffusivity ($D_{eff}$) and Sieverts' constant ($K_{S,eff}$). The dependence of the hydrogen diffusivity in PH-CuCrZr ELBRODUR® alloy and DS-GlidCop® Al25 alloy with temperature (shown in *Figure 8*) evidences the influence of trapping that provokes a general decrease in the diffusivity; i.e. the kinetics of migration becomes slower because trapping and detrapping processes impede the free flow of interstitial atoms through lattice solution sites. This effect becomes more pronounced as the temperature is lower (the vibration state of the hydrogen atom is weaker and the high trapping energy well is more effective for hydrogen trapping). At high temperatures, the diffusivity tends to approximate asymptotically to the behaviour of the base material Cu (curve 4) when the trapping effect becomes negligible. The alloys exhibit high values of diffusion energy (65.5 kJ/mol and 76,8 kJ/mol) and a marked influence of the trapping phenomenon with high values of trapping energies (51.2 kJ/mol and 75.4 kJ/mol). In the case of the in PH-CuCrZr ELBRODUR® alloy, the abundant hydrogen trapping sites in this material may be identified with the nanometric Guinier-Preston zones, incoherent pure Cr particles or extensive precipitates like $Cu_4Zr$ characteristic of this kind of alloy (Edwards et al., 2007). This behaviour is analogous to the trapping phenomena described in Gildcop Al25 (Esteban et al, 2009), where the presence of nanometric $Al_2O_3$ provoked a massive hydrogen trapping phenomenon even more effective than in the PH-CuCrZr alloy.
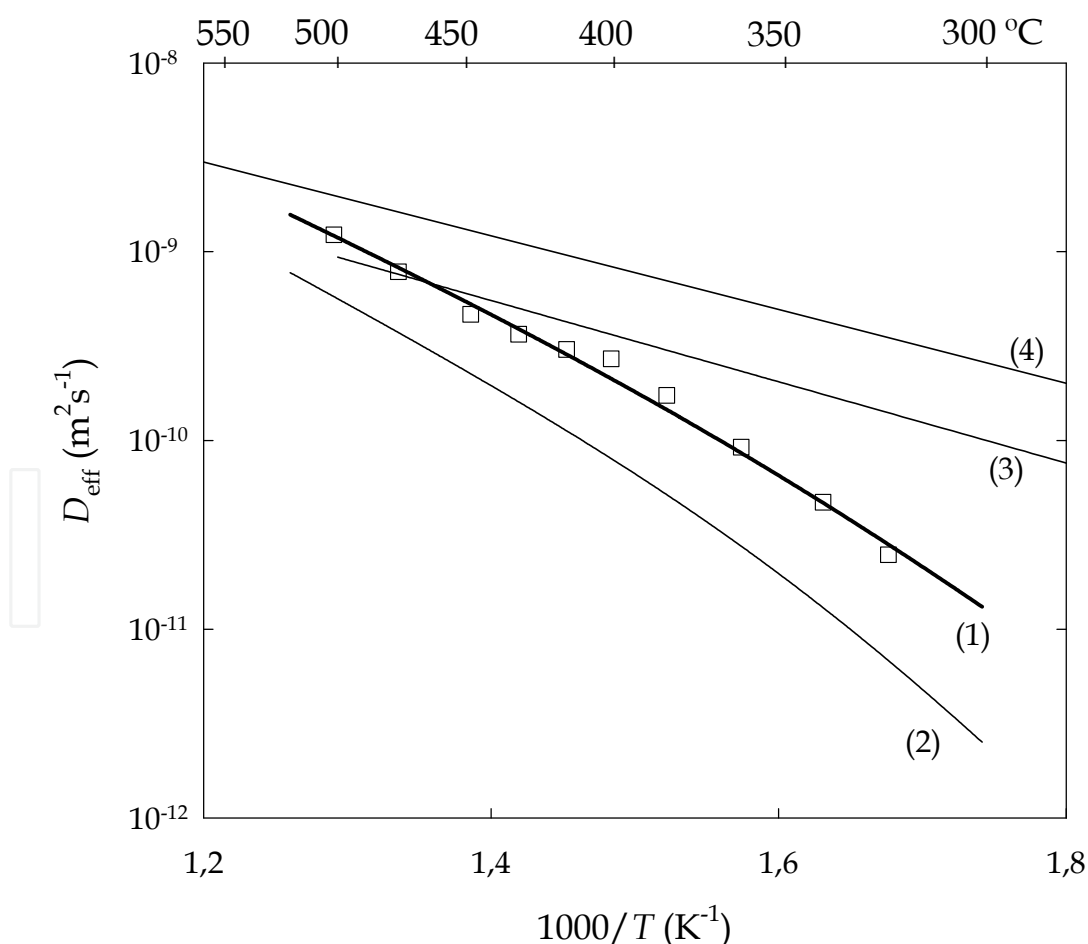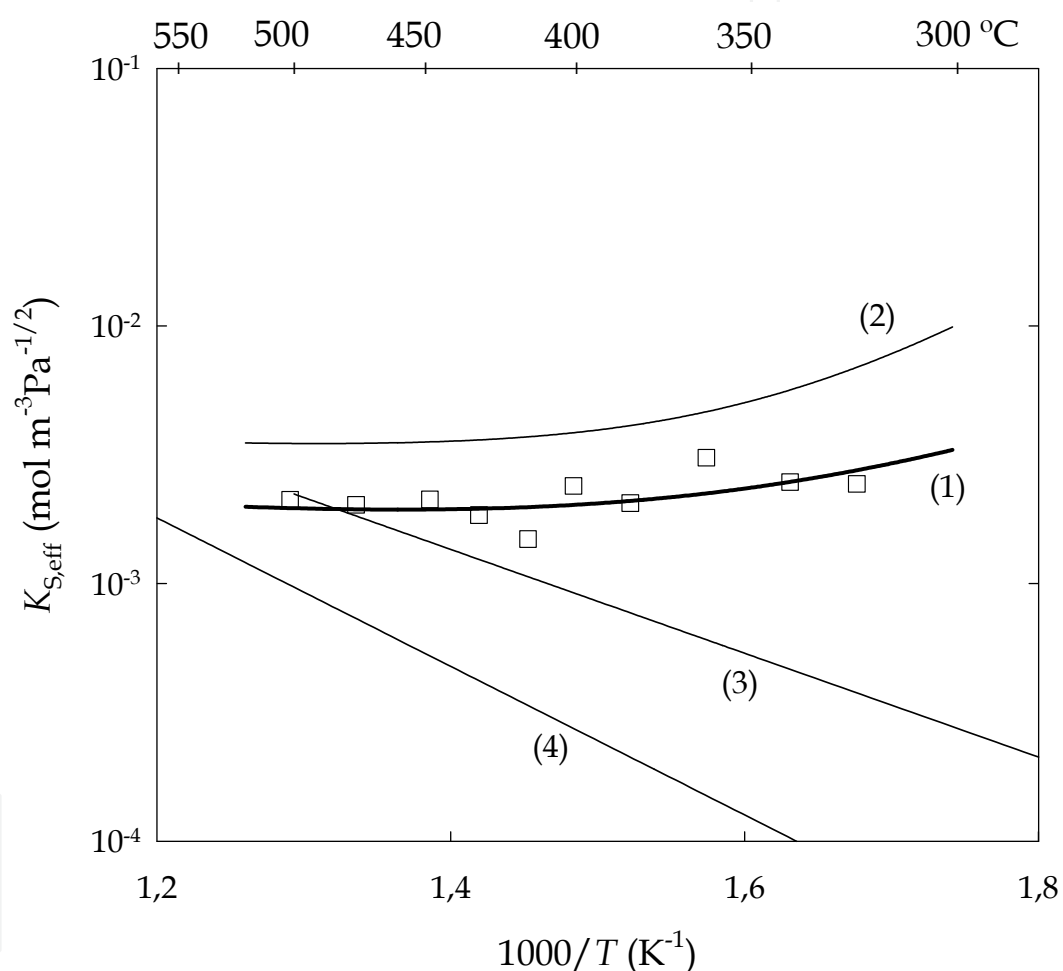


Fig. 8. Hydrogen diffusivity in PH-CuCrZr ELBRODUR® alloy compared with reference copper alloys: (1) ELBRODUR®, (2) GlidCop® Al25, (3) ELBRODUR-II, (4) pure Cu.

The hydrogen Sieverts' constants for the PH-CuCrZr ELBRODUR® alloy and the DS-GlidCop® Al25 alloy are shown in *Figure 9* in comparison to the base material, Cu. All over again, a marked trapping effect in hydrogen Sieverts' constant (i.e. solubility) has been observed throughout the whole temperature range for both alloys (curves 1 and 2). At low temperatures, hydrogen remains trapped into the defects of material exceeding the prediction made by the consideration of normal interstitial lattice sites of the base material Cu (curve 4). The interstitial lattice dissolution remains endothermic but with a low value of the dissolution energy for both alloys (8.4 kJ/mol and 3.7 kJ/mol). The trapped hydrogen specie becomes so important at low temperature that the effective Sieverts' constant behaves as an effective endothermic tendency.



Fig. 9. Hydrogen Sieverts´ constant in PH-CuCrZr ELBRODUR® alloy compared with reference copper alloys: (1) ELBRODUR®, (2) GlidCop® Al25, (3) ELBRODUR-II, (4) pure Cu.

The explanation of these particular tendencies may be found in the presence of high density nanosized defects in the materials. In the case of PH-CuCrZr ELBRODUR® alloy, the hydrogen interstitial atoms may remain trapped in the interface of the Guinier-Preston zones, incoherent Cr particles or precipitates, increasing the solubility and slowing down the transport through the lattice of the material (i.e. a lower effective diffusivity). In the case of the DS-GlidCop® Al25 alloy, the same effect can be attributed to the hydrogen inventory trapped in the nanosized $Al_2O_3$ particles. Furthermore, this phenomenon has been

experimentally identified in other kind of materials like oxide dispersion strengthened (ODS) reduced activation ferritic martensitic (RAFM) steels where nanoparticles of yttria $Y_2O_3$ provoked an analogous effect (Esteban et al., 2007).

The effect of nanosized inclusions has an obvious successful effect in the improvement of thermal-mechanical properties of copper alloys. However, the effect of the increase of hydrogen isotope inventory retention needs to be taken into account. This effect can be extremely important in particular cases. In fusion reactor materials, for example, it should be taken into account when choosing the structural and heat-sink materials of the fusion reactor where the hydrogen isotope inventory has to be controlled with special attention when considering fuel balance economy or radiological safety issues. When choosing materials for pipelines that will transport gaseous fuels including those with high hydrogen content or even pure hydrogen, the observed hydrogen trapping should be taken into account as long as it may degrade its mechanical properties. On the other hand, electrical characteristics may also be affected by hydrogen trapping phenomenon (Lee K. & Lee Y.K., 2000).

## 5. Conclusion

The gas permeation technique has been used in order to characterise two copper alloys proposed for high heat flux components: an oxide dispersion strengthened (DS) copper alloy named GlidCop® Al25, and a precipitation hardened (PH) copper alloy named ELBRODUR®. The hydrogen diffusive transport parameters have been obtained and discussed in relation to the particular microstructure of each copper alloy. The hydrogen trapping phenomenon has resulted to be present throughout the whole experimental temperature provoking an increase of hydrogen Sieverts' constant and decrease of diffusivity. The permeability values remained close to the values of the base material, i.e. pure Cu, and the other reference copper alloys. The analogy of the experimental results obtained with other materials with nanosized inclusions, confirms the high ability of these kinds of material to trap hydrogen isotopes at low temperatures. This should be monitored with special care for applications where hydrogen trapping may modify the physical properties of copper alloys.

## 6. Acknowledgment

## 7. References

Barabash V., (the ITER International Team), Peacock, A., Fabritsiev, S., Kalinin, G., Zinkle S., Rowcliffe, A., Rensman, J.-W., Tavassoli, A.A., Marmy, P., Karditsas P.J., Gillemot, F. & Akiba, M. (2007). Materials Challenges for ITER – Current Status and Future Activities. *Journal of Nuclear Materials*, Vol. 367-370, Part 1 (August 2007), pp. 31-32, ISSN-0022-3115

Carslaw, H. S. & Jaeger, J. C. (1959) *Conduction of Heat in Solids*, (2nd Edition), Clarendon Press, ISBN-0-19-853368-3, Oxford.

Edwards, D. J., Singh B. N., & Tähtinen S. (2007). Effect of heat treatments on precipitate microstructure and mechanical properties of a CuCrZr alloy. *Journal of Nuclear Materials*, Vol. 367-370, Part 2 (August 2007), pp. 904-909, ISSN-0022-3115

Esteban, G. A., Sedano, L. A., Perujo A., Douglas K., MAncinelli B., Ceroni P.l., Cueroni G.B. (1999). Hydrogen Transport Parameters and Trapping Effects in the Martensitic Steel Optifer-IVb. Report EUR 18995 EN (1999).

Esteban, G. A., Perujo A, Sedano, L. A., Legarda, F. Mancinelli, B. & Douglas, K. (2002). Diffusive transport parameters and surface rate constants of deuterium in Incoloy 800. *Journal of Nuclear Materials*, Vol. 300, Iss. 1 (January 2002), pp. 1-6, ISSN-0022-3115

Esteban, G. A., Perujo A, & Legarda, F. (2004). Tritium Management in the First-Wall Materials of A-DC and TAURO Blankets. *Journal of Nuclear Materials*, Vol. 335, Iss. 3 (December 2004), pp. 353-358, ISSN-0022-3115

Esteban, G. A., Peña, A., Legarda, F. & Lindau, R. (2007). Hydrogen Transport and Trapping in ODS-EUROFER. *Fusion Engineering and Design*, Vol. 82, Iss. 15-24 (October 2007), pp. 2634-2640, ISSN-0920-3796

Esteban, G. A., Alberro, G., Peñalva, I., Peña, A., Legarda, F. & Riccardi, B. (2009). Hydrogen Transport and Trapping in the GlidCop® Al25 IG Alloy. *Fusion Engineering and Design*, Vol. 84, Iss. 2-6 (June 2009), pp. 757-761, ISSN-0920-3796

Fabritsiev, S.A. & Pokrovsky, A.S. (2005). Effect of high doses of neutron irradiation on physico-mechanical properties of copper alloys for ITER applications. *Fusion Engineering and Design*, Vol. 73, Iss. 1 (April 2005), pp. 19-34, ISSN-0920-3796

ITER Doc. (2001). *ITER Materials Assessment Report (MAR)*, ITER Doc. G 74 MA 10 01-07-11 W0.2 (internal project document distributed to the ITER Participants).

Lee K. & Lee Y.K., (2000), Irreversible hydrogen effects on resistivity of sputtered copper films. *Journal of Materials Science*, Vol. 35. (May 2000), pp.6035-6040

Lorenzetto, P., Peacock, A., Bobin-Vastra, I., Briottet L., Bucci, P., Dell'Orco, G., Ioki, K., Roedig, M. & Sherlock, P. (2006). EU R&D on the ITER First Wall. *Fusion Engineering and Design*, Vol. 81, Iss. 1-7 (February 2006), pp. 355-360, ISSN-0920-3796

Meyder, R., Boccaccini, L. V. & Bekris, N. (2006) Tritium analysis for the European HCPB TBM in ITER, Proceedings of IEEE/NPSS 21st Symposium on Fusion Engineering, ISBN- 0-4244-0150-X, pp. 267-270, Knoxville, TN USA, September 2005

Möller W., (1984). Physics of Plasma-Wall Interaction in Controlled Fusion, NATO AISI series, p. 439, (1994)

Oriani R.A. (1970). The Diffusion and Trapping of Hydrogen in Steel, *Acta Metallurgica,* Vol. 18, (January 1970) , pp. 147-157

Reiter, F., Forcey, K.S. & Gervasini, G. (1993). A Compilation of Tritium-Material Interaction Parameters in Fusion Reactor Materials. Report EUR 15217 EN (1993).

Serra, E. & Perujo, A. (1998). Hydrogen and Deuterium Transport and Inventory Parameters in a Cu-0.65Cr-0.08Zr Alloy for Fusion Reactor Applications, *Journal of Nuclear Materials*, Vol. 258-263, Part 1 (October 1998), pp. 1028-1032, ISSN-0022-3115

Vykhodets, V. B., Geld, P. V., Demin, V. B. Men, A. N., Murtazin, I. A. & Fishman A. Ya. (1972). Isotope effect in the Solubility of Hydrogen in FCC Metals. *Physica Status Solidi (a)*, Vol. 9, Iss. 1, (January 1972), pp. 289-300, ISSN-1862-6319

Zinkle, S. J. & Fabritsiev S. A. (1994). Copper alloys for high heat flux application. *Atomic and Plasma-Material Interaction Data for Fusion*. Vol 5 (December 1994), pp. 163-191.
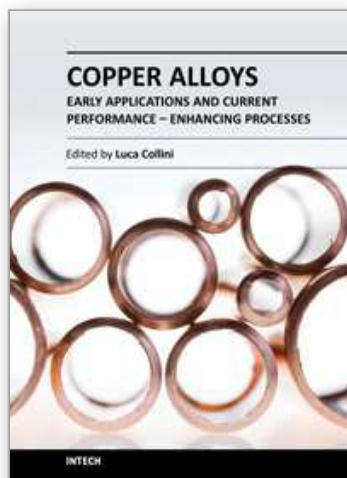
**Copper Alloys - Early Applications and Current Performance - Enhancing Processes**
Edited by Dr. Luca Collini

Copper has been used for thousands of years. In the centuries, both handicraft and industry have taken advantage of its easy castability and remarkable ductility combined with good mechanical and corrosion resistance. Although its mechanical properties are now well known, the simple f.c.c. structure still makes copper a model material for basic studies of deformation and damage mechanism in metals. On the other hand, its increasing use in many industrial sectors stimulates the development of high-performance and high-efficiency copper-based alloys. After an introduction to classification and casting, this book presents modern techniques and trends in processing copper alloys, such as the developing of lead-free alloys and the role of severe plastic deformation in improving its tensile and fatigue strength. Finally, in a specific section, archaeometallurgy techniques are applied to ancient copper alloys. The book is addressed to engineering professionals, manufacturers and materials scientists.

**How to reference**
In order to correctly reference this scholarly work, feel free to copy and paste the following:

I. Peñalva, G. Alberro, F. Legarda,G. A. Esteban and B. Riccardi (2012). Interaction of Copper Alloys with Hydrogen, Copper Alloys - Early Applications and Current Performance - Enhancing Processes, Dr. Luca Collini (Ed.), ISBN: 978-953-51-0160-4, InTech, Available from: http://www.intechopen.com/books/copper-alloys-early-applications-and-current-performance-enhancing-processes/interaction-of-copper-alloys-with-hydrogen

# INTECH
open science | open minds